Geometric Distortions in Side-Scan Sonar Images: A Procedure for Their Estimation and Correction

Daniel T. Cobra, *Member, IEEE*, Alan V. Oppenheim, *Fellow, IEEE* and Jules S. Jaffe, *Associate Member, IEEE*

Abstract—**A new procedure is introduced for the estimation and correction of geometric distortions frequently observed in side-scan sonar images as a result of motion instabilities of the sonar towfish. This procedure estimates geometric distortions from the image itself, without requiring navigational or attitude measurements. Estimates of the local degree of geometric distortion are obtained by cross-correlating segments of adjacent lines of the image. A mathematical model for the distortions is derived from the geometry of the problem and is applied to these estimates to reconstruct the sampling pattern on the seabed, under the assumption of a planar bottom. The estimated sampling pattern is then used for resampling the image to correct the geometric distortions. The model parameters may also be used for calculating approximate estimates of the attitude parameters of the towfish. A simulation is employed to evaluate the effectiveness of this technique and examples of its application to high-resolution side-scan sonar images are provided.**

Keywords—**Image processing, geometric distortion, side-scan sonar.**

I. Introduction

THE development of diving and submersible technology has made the bottom of the sea and other bodies of water stages for a large variety of enterprises, generating an increasing need for underwater remote sensing. In the aquatic environment, sonar provides remote sensing at ranges far beyond those afforded by optical means, and has acquired an important role in underwater exploration. Side-scan sonar provides acoustic imaging of the bottom at rates of up to several thousand square kilometers a day. Its wide range of applications includes mapping the seabed as an aid to the production of nautical charts and for oceanographic and underwater archeologic research, search and location of objects on the bottom, fishery studies, support for submersible operations, and off-shore mining and engineering surveys. A review of the history, principles of operation, and applications of side-scan sonar can be found in [1].

Manuscript received May 10, 1991; revised March 16, 1992. This work was sponsored in part by the Brazilian Government through the Conselho Nacional de Desenvolvimento Científico e Tecnológico (CNPq), in part by the Defense Advanced Research Projects Agency monitored by the Office of Naval Research under Grant N00014-89-J-1489, and in part by Lockheed-Sanders, Inc.

D. Cobra was with the Joint Program in Oceanography and Oceanographic Engineering of the Massachusetts Institute of Technology, Cambridge, MA, and the Woods Hole Oceanographic Institution, Woods Hole, MA. He is presently with the Departmento de Engenharia Elétrica at the Universidade de Brasília, Brasília, DF 70910, Brazil.

A. Oppenheim is with the Research Laboratory of Electronics at M.I.T., Cambridge, MA 02139.

J. Jaffe is with the Marine Physical Laboratory at the Scripps Institution of Oceanography, LaJolla, CA 92093.

IEEE Log Number 9201778.

A. Distortions in Sonographs

Fig. 1 shows a side-scan sonar image, also known as a *sonograph*. Such images are often affected by two kinds of distortions: intensity distortions, which are deviations from the ideal linear relation between image intensity and backscattering strength of the materials on the bottom, and geometric distortions, which correspond to discrepancies between the relative location of features on the image and their true location on the seabed. Various specific types of distortions can be identified in each of these two categories [2]–[4].

Geometric distortions in sonographs are caused by a number of different sources. One of them, the so-called *slant-range effect*, is inherent to side-scan sonar, and is a consequence of the cross-track coordinate of sonographs being range to the sonar towfish rather than horizontal distance on the bottom [5]. Another source of geometric distortions is variations of the speed of sound in the water, caused by differences in water temperature, pressure, or salinity. Gradients in the velocity of sound in the water cause the sound waves to be refracted, a phenomenon known as ray bending [6], [7]. Distortions caused by changes in the velocity of sound are usually observed only at longer ranges and are less common in high-frequency sonographs.

An important source of geometric distortion in sonographs is variations in the trajectory, speed, or orientation of the towfish. It is this type of geometric distortion that the techniques presented in this article seek to estimate and correct. Ideally, the towfish would be towed above the bottom at a constant speed, on a straight path, and with the heading always aligned with the trajectory. In practice, however, the towfish is often subject to motion instabilities. Its speed and course may vary, for instance, as a result of the effect of wind and sea currents on the deploying vessel, causing variations in aspect-ratio and other large-scale geometric distortions in the image. Geometric distortions may also be caused by the action of

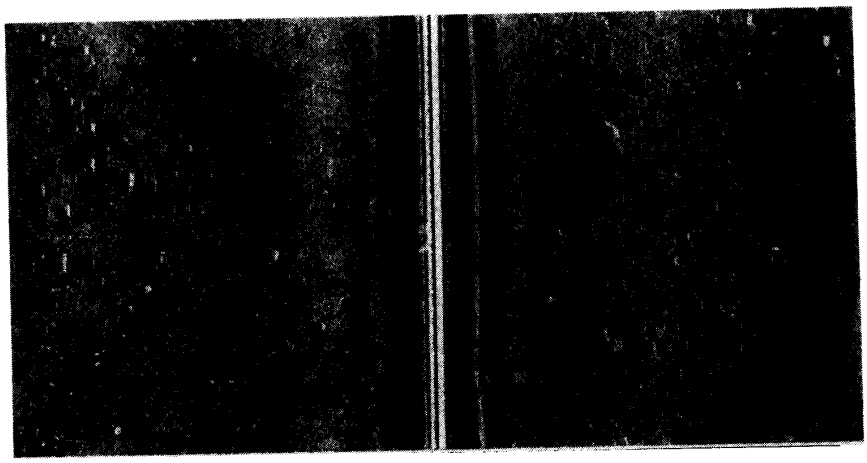

Fig. 1. Example of a side-scan sonar image, covering an area of 100 × 200 m of a fairly flat stretch of seabed consisting of a field of boulders with cables laid on the bottom.

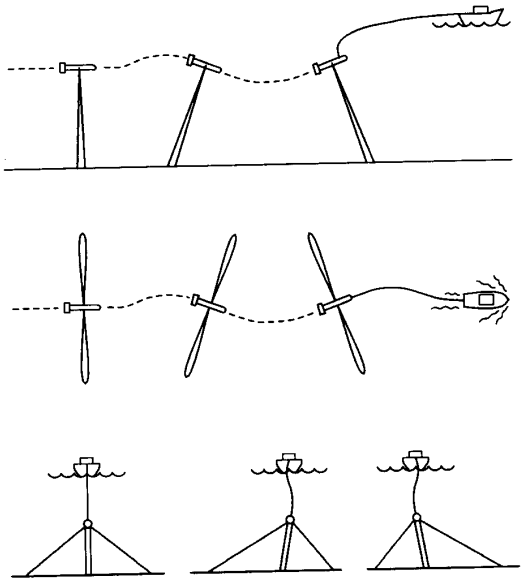

Fig. 2. Rotational instabilities of the towfish: pitching and yawing produce geometric distortions by causing the beams to scan ahead or back, either simultaneously on both sides, in the case of pitching (top), or alternately on the port and starboard sides, in the case of yawing (middle); rolling (bottom) does not produce geometric distortions, since it only causes the beam to rotate within its own plane.

underwater currents on the towfish itself or by the ship sway communicated to the towfish through the tow cable.

Motion instabilities may be divided into two types: translational and rotational. Translational instabilities correspond to lateral and vertical displacement of the towfish from the desired straight path, and to variations in speed. Rotational instabilities are illustrated in Fig. 2. Pitching and yawing cause geometric distortions, while rolling may result in intensity distortions in the area immediately below the towfish and at the maximum range due to the rotation of vertical sidelobes. If pitching and yawing are severe enough, the sonar beam may scan backwards over a previously covered area. Objects in a backscanned area appear in triplicate on the sonograph: one image corresponding to the first time they were scanned, followed by their mirror image reversed in the along-track direction resulting from backscanning, and, finally, a third image produced when the beam starts scanning forward again.[1]

Marking the points on the seabed plane that correspond to points in the digitized image, we obtain sampling patterns such as those shown in Fig. 3. Fig. 3(a) depicts the ideal case where the towfish follows a straight trajectory at a constant speed and with no pitching or yawing. The scan lines on the bottom are bent forward because the receiving beam keeps moving ahead with the sonar during acquisition of each line. However, if the maximum range of the sonar is much larger than the spacing between scan lines in the along-track direction, which is usually the case, then the resulting sampling pattern approximates a rectangular grid. Fig. 3(b) indicates how the sampling pattern is distorted when the towfish is subject to translational and rotational instabilities. In this case, it may depart considerably from the ideal rectangular grid, causing geometric distortions in the resulting image. In areas where the sampling distance is smaller the image will look "stretched" with respect to areas where the sampling distance is larger. The image will look skewed whenever scan lines are shifted in the cross-track direction.

B. Correction of Geometric Distortions in Sonographs

For about a decade after the invention of side-scan sonar, the only types of geometric distortions that were corrected were those caused by variations in ship speed and by the slant-range effect. More advanced techniques

[1] Towfish instabilities do not produce backscanning in the cross-track direction, since they cannot cause the propagating wavefront to reverse its course.

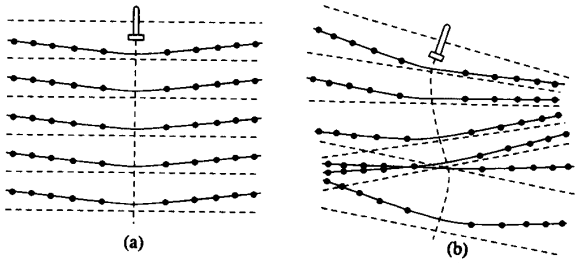

Fig. 3. Top view of sampling patterns on the bottom. Under ideal conditions (a) the scan lines are slightly curved due to the forward motion of the towfish, and the sampling distance along each line varies according to the slant-range effect. When the towfish is subject to motion instabilities (b) the sampling distance between corresponding points of successive scan lines varies, producing geometric distortions. Scan lines may cross, resulting in backscanning.

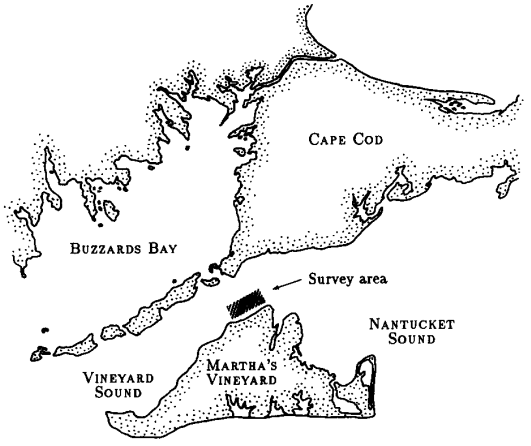

Fig. 4. A survey area was chosen where utility cables were known to be found on the bottom. Although the technique developed for corecting geometric distortions does not make any assumptions about or rely in any way on the presence of such objects in the image, such features facilitate the perception of geometric distortions and can provide some visual indication of the effectiveness of this technique in correcting them.

for correction of geometric distortions became available with the introduction of digital processing of sonographs. Paluzzi *et al.* [8] used existing software developed at the Jet Propulsion Laboratory of the California Institute of Technology for processing images from unmanned planetary exploration missions, and adapted it for sonograph processing. Their system employed navigational data for correction of large-scale geometric distortions and production of sonograph mosaics. That software package was also used and extended by Luyendyk, Hajic, and Simonett at the University of California, Santa Barbara [9]. Similar sonograph-processing systems have since been developed at the National Mapping Division of the U.S. Geological Survey, as reported by Chavez in [4], and at France's Institut Français de Recherche pour l'Exploitation de la Mer, as reported by Augustin in [10]. Other instances of digital processing of sonographs that include correction of geometric distortions are described in [11]–[19].

Accurate correction of geometric distortions caused by towfish motion instabilities requires knowledge of the attitude parameters of the towfish during acquisition of the the image. These are available only in the case of a few more sophisticated units, equipped with attitude sensors. When attitude measurements are not available, geometric distortions have been corrected by assuming that the towfish follows the variations in course of the deploying vessel, which are determined from navigational measurements, and then by resampling the image accordingly. In this article, we present a new technique for correcting geometric distortions caused by towfish instabilities that requires neither navigational nor attitude measurements.

C. Experimental Methods

The sonographs shown in this article were collected during a survey conducted from the Woods Hole Oceanographic Institution (WHOI) on August 15, 1987. Fig. 4 shows the location of the surveyed area off the island of Martha's Vineyard, MA.

The survey was conducted aboard the R. V. Asterias with a high-resolution 500-kHz Klein model 422S-001E towfish and a Klein model 521 recorder operating at a maximum range of 100 m, the upper limit afforded by that high-frequency unit. The demodulated signal was recorded on magnetic tape and was later digitized through a personal-computer system equipped with a "frame-grabber" card. The sonar firing rate, the vessel speed, and the sampling rate were chosen to result in sampling distances of 20 cm in both the along-track and cross-track directions (in the absence of motion instabilities). Before digitization, the signal was filtered with a low-pass circuit of appropriate bandwidth, to prevent aliasing. The size of the digitized images is 512 × 1024 pixels, corresponding to an area of approximately 100 × 200 m. Though the sea condition during the survey could be described as only moderately rough, the small size of the vessel (46 ft, 20 long tons loaded displacement) resulted in enough swaying to generate a significant degree of geometric distortion in the images. To that was added the effect of fairly strong undercurrents prevailing in Vineyard Sound.

In Sections II–IV, we carry out the mathematical analysis of the problem and development of the algorithm. The estimation and correction of geometric distortions in the sample sonograph of Fig. 1 is presented in Section V. The reader may want to refer ahead to that section while progressing through Sections II–IV.

II. Mathematical Analysis of the Problem

A. Assumptions

A digitized sonograph can be viewed as a mapping onto a monochrome digital image of the backscattering strength of materials on the seabed. We denote the digital sonograph image by $s[m, n]$, where $[m, n]$ are the coordinates of the image matrix,[2] and the backscattering strength of the seabed by $b(x, y)$, where x and y are part of a

[2] The square brackets are used to indicate that m and n are discrete rather than continuous variables.

rectangular coordinate system (x, y, z) defined in the water, as illustrated in Fig. 5.[3]

In analyzing the geometry of the problem, we make the following assumptions.

- The bottom is assumed to be planar and horizontal (corresponding to the plane defined by $z = 0$). This assumption is commonly made for the correction of geometric distortions in sonographs, since in standard side-scan sonars variations in bottom elevation are undetermined for lack of information on the bearing of the returned signals.
- It is assumed that the wavefront propagates through the water at a constant speed and that ray-bending does not occur.
- The towfish roll angle is assumed to be zero, since, as pointed out in Section I.A, rolling does not contribute to geometric distortions.
- The towfish is assumed to remain stationary from the moment a pulse is fired until the return from the maximum range is received. This implies that the scan lines defined by the intersection of the beam pattern axial plane with the seabed plane are approximated by straight lines, as shown in Fig. 6. See [20] for an analysis that does not rely on this assumption, and is more suitable to long-range sonars operating at low firing rates.
- We assume that the sonograph has been processed to correct the slant-range distortion. This is a straightforward operation, assuming a planar bottom. Denoting by $\bar{s}[l, n]$ the original image and by $h[n]$ the height of the water column in pixels at the nth line, we have

$$s[m, n] = \bar{s}[l, n]|_{l=\sqrt{h^2[n]+m^2}} \tag{1}$$

for $m = 0, \pm 1, \cdots, \pm (N_M - 1)$ and $n = 0, 1, \cdots, N_n - 1$, where N_n is the number of (horizontal) lines in the slant-range corrected image and N_m is the number of pixels per line on each side. Since the value of l corresponding to m will in general be noninteger, this equation assumes the use of an appropriate technique for interpolating the lines of the original image at noninteger coordinates.

B. Geometric Framework

Ignoring intensity distortions, the mapping from backscattering strength on the bottom to points of the slant-range corrected image can be described by

$$s[m, n] = b(x, y)|_{\substack{x=x_s[m,n] \\ y=y_s[m,n]}},$$

where $x_s[m, n]$ and $y_s[m, n]$ are the coordinates of the point on the seabed that was sampled to produce the pixel located at $[m, n]$ in the image. To correct geometric distortions in the sonograph, it is necessary to determine the inverse mapping $[m, n] \mapsto (x, y)$.

[3] $b(x, y)$ is the backscattering strength for the particular incident angle at which the wavefront reaches point (x, y).

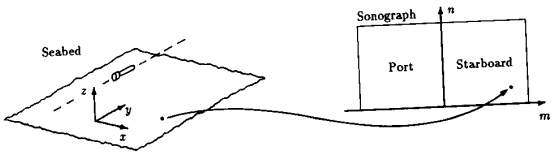

Fig. 5. Coordinate systems defined on the seabed and on the sonograph. The coordinate system defined on the seabed plane may, in principle, have any arbitrary orientation. However, it is useful to align the y direction with the trajectory of the towfish, as shown here, so that it may be referred to as the along-track direction and x as the cross-track direction. In the sonograph, the n direction is defined to point up, coinciding with the direction of scanning, while m is defined to be positive on the starboard (right) side and negative on the port (left) side of the image.

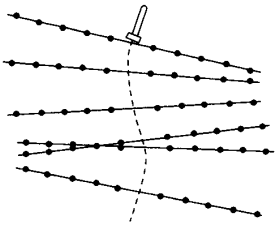

Fig. 6. By assuming that the towfish remains stationary between successive pulse firings, we approximate the scan lines on the bottom by straight lines. This results in a simpler model for the geometric distortions.

The geometry of the problem is depicted in Fig. 7. The projection of $(x_f[n], y_f[n], z_f[n])$ onto the line defined by the intersection of the beam plane and seabed plane defines the point $x_o[n], y_o[n])$ that will appear in equations derived later. The instant at which acquisition of the sonograph was initiated corresponds to $n = 0$, and thus $(x_f[0], y_f[0], z_f[0])$ is the starting point of the towfish trajectory.

C. Sampling Displacements

Our measures of geometric distortion in sonographs are based on estimates of the differences in the values of $x_s[m, n]$ and $y_s[m, n]$ between sampling points at fixed values of m from one line of the image to the next. These differences are denoted by

$$\Delta_n x_s[m, n] \triangleq x_s[m, n + 1] - x_s[m, n]$$

$$\Delta_n y_s[m, n] \triangleq y_s[m, n + 1] - y_s[m, n]$$

and are illustrated in Fig. 8(a). We call them the *sampling displacements* in the cross-track and along-track directions, respectively. In the absence of geometric distortions, we have

$$x_s[m, n + 1] = x_s[m, n]$$

$$y_s[m, n + 1] = y_s[m, n] + vT_f$$

for all m and n, where v is the speed of the towfish and T_f

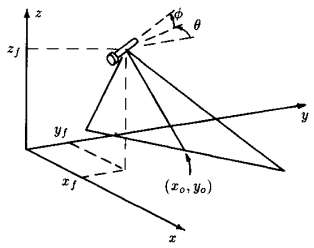

Fig. 7. The position of the towfish during acquisition of the nth line of the sonograph is $(x_f[n], y_f[n], z_f[n])$. Its orientation is described by the pitch angle, $\phi[n]$, corresponding to elevation measured with respect to the horizontal seabed plane, and yaw angle, $\theta[n]$, corresponding to azimuth measured from the y direction towards the port side.

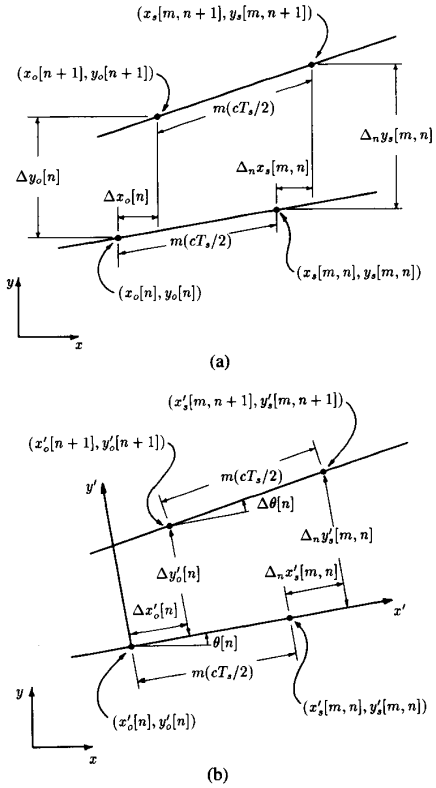

Fig. 8. Sampling displacements in the original coordinate system (x, y) (a) and in the auxiliary coordinate system (x', y') that follows the changes in towfish attitude (b).

the sonar firing period. Therefore,

$$\Delta_n x_s[m, n] = 0, \quad \Delta_n y_s[m, n] = vT_f.$$

Towfish instabilities cause $\Delta_n x_s[m, n]$ and $\Delta_n y_s[m, n]$ to depart from these values, producing geometric distortions.

It is useful to introduce an auxiliary rectangular coordinate system, (x', y'), shown in Fig. 8(b), with the x' axis located on the line defined by the intersection of the axial plane of the effective beam with the seabed plane, and with the y' axis pointing in the direction of the towfish heading during acquisition of the nth line. Thus, the axes of this new coordinate system are rotated with respect to the original coordinate system by an angle equal to $\theta[n]$ and its origin is translated to point $(x_o[n], y_o[n])$.

In the auxiliary coordinate system, the sampling displacements are denoted by $\Delta_n x'_s[m, n]$ and $\Delta_n y'_s[m, n]$. In Section III, we will consider how these quantities can be estimated from the image by cross-correlating segments of adjacent lines.

D. Linear Model for the Sampling Displacements

From Fig. 8 we see that

$$x_s[m, n] = x_o[n] + m(cT_s/2)\cos\theta[n] \tag{2a}$$

$$y_s[m, n] = y_o[n] + m(cT_s/2)\sin\theta[n] \tag{2b}$$

where c is the speed of sound in water and T_s is the (constant) sampling period used in digitizing the returned signals. The lines of the digitized image were interpolated to correct the slant-range distortion, as described in (1). Therefore, if the sampling points of the resulting image are plotted on the seabed, they are separated along each scan line by a *constant* distance $cT_s/2$.[4] The first-order Taylor-series expansion of (2a) and (2b) yields the following expressions for the sampling displacements:

$$\Delta_n x_s[m, n] \approx \Delta x_o[n] - m(cT_s/2)\sin\theta[n]\,\Delta\theta[n]$$

$$\Delta_n y_s[m, n] \approx \Delta y_o[n] + m(cT_s/2)\cos\theta[n]\,\Delta\theta[n]$$

where

$$\Delta x_o[n] \triangleq x_o[n+1] - x_o[n]$$

$$\Delta y_o[n] \triangleq y_o[n+1] - y_o[n]$$

$$\Delta\theta[n] \triangleq \theta[n+1] - \theta[n].$$

It is straightforward to show that in the (x', y') coordinate system these equations become

$$\Delta_n x'_s[m, n] \approx \Delta x'_o[n], \tag{3a}$$

$$\Delta_n y'_s[m, n] \approx \Delta y'_o[n] + m(cT_s/2)\,\Delta\theta[n], \tag{3b}$$

where $\Delta x'_o[n]$ and $\Delta y'_o[n]$ correspond to $\Delta x_o[n]$ and $\Delta y_o[n]$ in the (x', y') system.

With the linear model of (3a) and (3b), our task is now reduced to the estimation of three model parameters, namely $\Delta x'_o[n]$, $\Delta y'_o[n]$, and $\Delta\theta[n]$, for each line of the sonograph, from the estimates of sampling displacements. The resulting estimates of model parameters will then be used for estimating the sampling point coordinates for all points in the image. We will see in Section IV how that can be accomplished.

Fig. 9 illustrates the overall process of estimating the sampling point coordinates. First, the height of the water column is measured in the original sonograph $\bar{s}[l, n]$ and is then used for correcting the slant-range distortion to produce a new image $s[m, n]$, from which estimates of the sampling displacements $\Delta_n x'_s[m, n]$ and $\Delta_n y'_s[m, n]$ are

[4] cT_s is divided by 2 to account for the two-way travel time of the sound pulse.

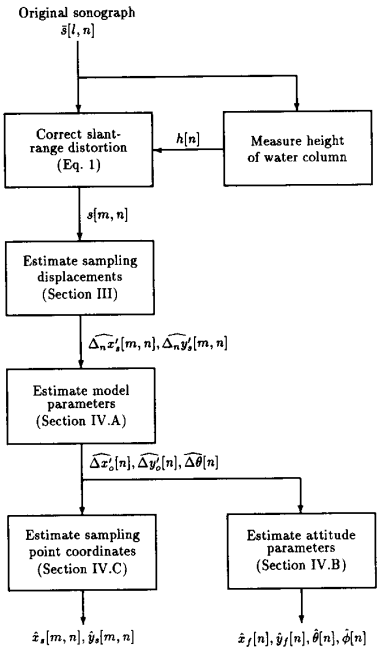

Fig. 9. Technique for estimating sampling point coordinates. (See explanation in the text.)

obtained by techniques introduced in Section III. In order to reduce the estimation error, the linear model of (3a) and (3b) is then applied to the estimates of sampling displacements, yielding estimates of the model parameters $\Delta x'_o[n]$, $\Delta y'_o[n]$, and $\Delta\theta[n]$. As indicated in the figure, it is possible to use these estimates for estimating in turn the towfish attitude parameters. Though this is not necessary for correcting the geometric distortions, it is convenient to obtain estimates of parameters that describe more directly the location and orientation of the towfish. From the estimates of model parameters, we obtain new estimates of the sampling displacements, which are converted to the (x, y) coordinate system and added recursively to yield the final estimates of sampling point coordinates, as we will see in Section IV.

III. Measures of Geometric Distortion in Sonographs

A. Assumptions on the Statistical Properties of the Image

Estimating geometric distortions in a songraph from the image alone requires that certain assumptions be made about the imaged scene. The basic assumption we make is that $b(x, y)$, the backscattering function of the seabed plane, is a two-dimensional wide-sense stationary random process with isotropic autocorrelation function, i.e., that the correlation between any two points of the seabed depends only on the distance between them. Thus, if $R_b(\Delta x, \Delta y; x, y)$ denotes the autocorrelation function of the backscattering function at point (x, y) and at lags $(\Delta x, \Delta y)$, we have

$$R_b(\Delta x, \Delta y; x, y) = R\left(\sqrt{(\Delta x)^2 + (\Delta y)^2}\right)$$

for some one-dimensional function $R(\ )$.

The assumption that the backscattering function is wide-sense stationary may not hold if there are significant variations in the morphology of the bottom. The assumption of isotropy is valid if there is no systematic orientation of the features on the bottom in some direction, but it may not hold in areas containing sand dunes or other formations shaped by undercurrents. However, the techniques presented here may still be applied in such cases if the image is divided into areas where the morphology is uniform enough for the assumptions of wide-sense stationarity and isotropy to be locally valid.

Based on the assumptions above, in the absence of geometric distortions the digitized sonograph is in turn assumed to be a two-dimensional wide-sense stationary discrete-space sequence with isotropic autocorrelation sequence. In that case, the shape of the autocorrelation sequence of small areas of the image is radially symmetric and is constant throughout the sonograph. However, when geometric distortions are present, the shape of the local autocorrelation sequence varies from one part of the image to another, reflecting the local degree and orientation of the geometric distortion. These variations provide our measures of geometric distortions in sonographs, as explained in the next sections.

B. Estimation of the Normalized Covariance Sequence

To account for local variations in the mean and standard deviation of the image intensity, we use a local normalized covariance sequence rather than the local correlation sequence. Denoting by $\mu_s[m, n]$ and $\sigma_s[m, n]$ the mean and standard deviation of the image at point $[m, n]$, the local normalized covariance sequence is defined as

$$\begin{aligned}\rho_s[\Delta m, \Delta n; m, n] &\triangleq E\{(s[m,n] - \mu_s[m,n]) \\ &\quad (s[m+\Delta m, n+\Delta n] - \mu_s[m+\Delta m, n+\Delta n])\} \\ &\quad /(\sigma_s[m,n]\sigma_s[m+\Delta m, n+\Delta n])\end{aligned}$$

where $E\{\ \}$ denotes the expected value.[5]

We estimate $\rho_s[\Delta m, \Delta n; m, n]$ through the sample correlation coefficient of a block of pixels centered at $[m, n]$ with respect to neighboring blocks. In principle, the averaging could be carried out over blocks extending over two or more lines of the image, but single-line segments are used because geometric distortions can be expected to cause greater variation in correlation in the along-track direction than in the cross-track direction, as a result of the raster-scan fashion in which the bottom is sampled. Assume that the line segment extends for M pixels on each side of the point being considered, as seen in Fig. 10. Then the local sample mean and standard deviation of the

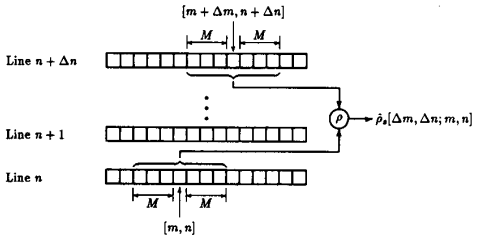

Fig. 10. The local normalized covariance sequence $\rho_s[\Delta m, \Delta n; m, n]$ is estimated by calculating the sample correlation coeffiecient between line segments of length $(2M + 1)$ separated by lags Δm and Δn.

image over that segment are

$$\hat{\mu}_s[m,n] = \frac{1}{2M+1}\sum_{k=-M}^{M} s[m+k,n]$$

$$\hat{\sigma}_s[m,n] = \left[\frac{1}{2M+1} \cdot \sum_{k=-M}^{M} (s[m+k,n] - \hat{\mu}_s[m,n])^2\right]^{1/2}$$

and the sample normalized covariance sequence is given by

$$\hat{\rho}_s[\Delta m, \Delta n; m, n] = \frac{1}{2M+1}\left[\sum_{k=-M}^{M} (s[m+k,n] - \hat{\mu}_s[m,n])(s[m+\Delta m+k, n+\Delta n] - \hat{\mu}_s[m+\Delta m, n+\Delta n])\right] / (\hat{\sigma}_s[m,n]\hat{\sigma}_s[m+\Delta m, n+\Delta n]).$$

C. Estimation of Sampling Displacements in the Cross-Track Direction

In lines of the sonograph where the towfish was subject to lateral displacements (i.e., in the x' direction) the normalized covariance sequence $\rho_s[\Delta m, \Delta n; m, n]$ becomes skewed in the cross-track direction, and its contour lines, which would be concentric circles in the absence of geometric distortions, become elliptical, as shown in Fig. 11(a). The displacement of the maximum point of the sample sequence $\hat{\rho}_s[\Delta m, \Delta n; m, n]$ at a lag $\Delta n = 1$ is used as an indicator of how much line $(n + 1)$ of the image was shifted relative to line n at a cross-track coordinate m, therefore providing an estimate of the sampling displacement $\Delta_n x_s'[m, n]$, as shown in Fig. 11(b). Thus

$$\widehat{\Delta_n x_s'}[m,n] = -\frac{cT_s}{2}\arg\max_{\Delta m}\hat{\rho}_s[\Delta m, 1; m, n].$$

[5] Notice that $\rho_s[\Delta m, \Delta n; m, n]$ is the correlation coefficient between $s[m, n]$ and $s[m + \Delta m, n + \Delta n]$.

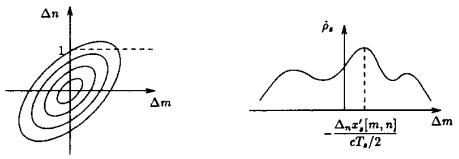

Fig. 11. Lateral displacements of the towfish cause the local covariance sequence of the image to become skewed. The displacement of the maximum point of the sample covariance sequence at a lag $\Delta n = 1$ provides the estimate of the sampling displacement in the cross-track direction, $\Delta_n x_s'[m, n]$.

The $(cT_s/2)$ factor is again required for the conversion from m (image coordinates in pixels) to x' (distances on the seabed in meters), and the negative sign is included because if line $(n + 1)$ of the image seems to be shifted in one direction with respect to line n, then the sampling points must have shifted in the opposite direction on the bottom from one scan to the next. To avoid coarse quantization of the estimates of sampling displacement, the lines of the image are upsampled (i.e., their number of samples is increased through band-limited interpolation) before the local normalized covariance sequence is computed.

D. Estimation of Sampling Displacements in the Along-Track Direction

In the along-track direction, distortions are caused by variations in the towfish speed and by pitching and yawing, which affect the sampling distance on the bottom by disturbing the constant pace at which the sonar beam would ideally move. As a result, the image looks "stretched" in areas where the sampling distances are smaller and "compressed" in areas where they are longer. A similar effect is observed in the shape of the local autocorrelation sequence of the image, as indicated in Fig. 12(a). The width of the main peak of the local sample normalized covariance sequence at $\Delta m = 0$ reflects the distortions in the along-track direction by becoming narrower or wider in different areas of the image. In our algorithm, the width of the main peak is measured through the correlation lengths $L_n^+[m, n]$ and $L_n^-[m, n]$, which are defined to be the lags at which $\hat{\rho}_s[0, \Delta n; m, n]$ falls to a given threshold ρ_o, as illustrated in Fig. 12(b). Thus we have

$$\hat{\rho}_s[0, L_n^+[m,n]; m, n] = \rho_o$$
$$\hat{\rho}_s[0, -L_n^-[m,n]; m, n] = \rho_o.$$

This time the columns of the image are upsampled before the correlation lengths are calculated, to avoid coarse quantization.

Relating Correlation Lengths to Sampling Displacements: Obtaining estimates of sampling displacements in the along-track direction from the local sample normalized covariance sequence is complicated by the fact that the width of the main peak of $\hat{\rho}_s[\Delta m, \Delta n; m, n]$ is not directly related to $\Delta_n y_s'[m, n]$, but rather to the sampling distance,

$$P_n[m,n] \triangleq \sqrt{(\Delta_n x_s'[m,n])^2 + (\Delta_n y_s'[m,n])^2} \quad (4)$$

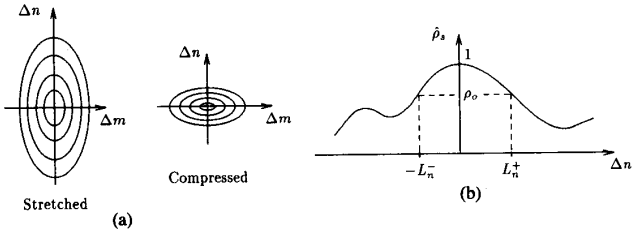

Fig. 12. Stretching and compression of the image in the along-track direction are reflected on the shape of the local sample covariance sequence. The positive- and negative-lag correlation lengths, $L_n^+[m,n]$ and $L_n^-[m,n]$, are measures of the width of the main peak of the sequence with respect to a given threshold ρ_o.

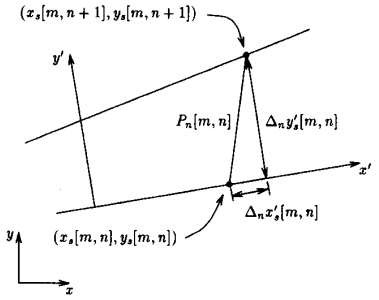

Fig. 13. Correlation lengths are related to the distance $P_n[m,n]$ that separates corresponding points of adjacent scan-lines (i.e., points with same range coordinate m).

illustrated in Fig. 13. Thus, to obtain a direct measure of $\Delta_n y_s'[m,n]$, we first process the image to make $\Delta_n x_s'[m,n]$ approximately equal to zero. To that end we calculate the estimates $\widehat{\Delta_n x_s'}[m,n]$ as described in the preceding section. Then, starting from the bottom of the image, we compute the average value of $\widehat{\Delta_n x_s'}[m,n]$ for each line and shift the line above it by the corresponding number of pixels in the opposite direction. Since the desired shift in general corresponds to a noninteger number of pixels, it is accomplished by adding to the Fourier transform of the line the appropriate phase shift and then taking the inverse transform. We thus assume that $\Delta_n x_s'[m,n]$ has been reduced to zero in the resulting image, so that (4) becomes

$$P_n[m,n] = |\Delta_n y_s'[m,n]|. \tag{5}$$

Let us consider for now only positive-lags, for the sake of simplicity. Let $L_b[m,n]$ denote the correlation length of the seabed backscattering function $b(x,y)$ at point $(x_s[m,n], y_s[m,n])$. Since $b(x,y)$ is assumed to be isotropic, its correlation length equals $L_b[m,n]$ in all directions. We have seen that $L_n^+[m,n]$ is the number of pixels that we have to travel from point $[m,n]$ in the positive n dirction before the local sample covariance sequence of the image drops to the threshold ρ_o. Similarly, $L_b[m,n]$ is the distance the sonar beam has to travel on the seabed from point $(x_s[m,n], y_s[m,n])$ before the local normalized covariance function of $b(x,y)$ falls to that same threshold. Thus, assuming for now that $L_n^+[m,n]$ is an integer number of pixels (that is, that the columns of the image are not upsampled), $L_b[m,n]$ equals the sum of the $L_n^+[m,n]$ next sampling distances $P_n[m,n]$ from point $(x_s[m,n], y_s[m,n])$, i.e.,

$$L_b[m,n] = \sum_{i=0}^{L_n^+[m,n]-1} P_n[m,n+i]. \tag{6}$$

Incidentally, notice that this equation may also be written as

$$L_b[m,n] = L_n^+[m,n]\bar{P}_n^+[m,n]$$

where $\bar{P}_n^+[m,n]$ represents the average of the $L_n^+[m,n]$ sampling distances after point $[m,n]$. Thus, if $L_b[m,n]$ is constant, or at least fairly uniform throughout the sonograph, then, as expected, the positive-lag correlation length at point $[m,n]$ is inversely proportional to the sampling distance, or, more accurately, to the average of the $L_n^+[m,n]$ sampling distances immediately after that point.

Now, let $L_{no}[m]$ represent the average value of the correlation lengths over all lines of the image if it were not affected by geometric distortions.[6] In the absence of motion instabilities the sampling periods equal vT_f and (6) yields

$$L_b[m,n] = vT_f L_{no}[m].$$

Substituting this expression and (5) into (6) we obtain

$$vT_f L_{no}[m] = \sum_{i=0}^{L_n^+[m,n]-1} |\Delta_n y_s'[m,n+i]|. \tag{7}$$

This is the desired expression relating the correlation lengths, $L_n^+[m,n]$, to the sampling displacements in the along-track direction, $\Delta_n y_s'[m,n]$.

For convenience, we define

$$q[m,n] \triangleq \frac{|\Delta_n y_s'[m,n]|}{vT_f L_{no}[m]}. \tag{8}$$

[6] Strictly speaking, the average correlation length should be denoted $L_{no}[l]$, since the sonar beam pattern causes it to vary with range rather than with the horizontal distance on the bottom. However, we denote it by $L_{no}[m]$ for the sake of simplicity, with the conversion from l to m left implicit. Also, no superscript is used in $L_{no}[m]$ because it represents the averages of both $L_n^+[m,n]$ and $L_n^-[m,n]$, which are equal if there is no geometric distortion.

Furthermore, we have assumed for simplicity that the correlation lengths are intergers. However, as previously mentioned, the columns of the image are upsampled so that the correlation lengths may be calculated more precisely, being, in general, noninteger. Equation (7) may be written in terms of the $q[m,n]$ and modified to accommodate noninteger values of $L_n^+[m,n]$ as

$$(L_n^+[m,n] - \lfloor L_n^+[m,n]\rfloor)q[m,n+\lfloor L_n^+[m,n]\rfloor] + \sum_{i=0}^{\lceil L_n^+[m,n]\rceil - 1} q[m,n+i] = 1 \quad (9)$$

where $\lfloor L_n^+[m,n]\rfloor$ denotes $L_n^+[m,n]$ rounded towards zero. The term outside the sum accounts for the fractional part of $L_n^+[m,n]$. Similarly, for the negative-lag correlation lengths, we have

$$(L_n^-[m,n] - \lfloor L_n^-[m,n]\rfloor)q[m,n-\lfloor L_n^-[m,n]\rfloor] + \sum_{i=0}^{\lfloor L_n^-[m,n]\rfloor - 1} q[m,n-i] = 1. \quad (10)$$

At each cross-track coordinate m, (9) and (10) provide a set of $2(N_n - 1)$ independent linear equations in the $(N_n - 1)$ unknowns,[7] $q[m,n]$, $n = 0,1,2,\cdots,N_n - 2$. The least squares solution of this overdetermined system provides the estimates $\hat{q}[m,n]$. This procedure may be interpreted as an inverse filtering operation that compensates for the time-varying averaging implied by (9) and (10).

We now have estimates of the quantities $q[m,n] \triangleq |\Delta_n y_s'[m,n]|/vT_f L_{no}[m]$. In order to obtain the desired estimates of the sampling displacements $\Delta_n y_s'[m,n]$, it is necessary to estimate $L_{no}[m]$, i.e., what the correlation lengths should be in the absence of geometric distortions, and to remove the absolute value operation.

Correlation Lengths in the Absence of Geometric Distortion: The correlation lengths are affected by the composition of the seabed in the area scanned to form the sonograph. In fact, measures similar to the correlation lengths defined here have been used for the prupose of classifying different types of geological formations on the bottom, such as sand dunes, rock outcrops, mud, gravel, etc. [21]. It is therefore necessary to know the correlation lengths associated with the different kinds of materials appearing in a sonograph, if one is to use variations in the correlation length as a measure of geometric distortion. The correlation lengths are also affected by the sonar beam pattern, since the sonograph image is formed by the convolution of the beam pattern with the backscattering function of the seabed. The beam pattern becomes wider at longer ranges, causing a corresponding increase in the correlation lengths.

To estimate $L_{no}[m]$ we first choose a set $\mathcal{N}$ of lines from the sonograph where visual inspection does not indicate geometric distortion, and where the bottom morphology appears to be fairly uniform, so that the average correlation length may be a function of m only. On those lines we assume that $\Delta_n y_s'[m,n] = vT_f$, so that, from (8), we have $q[m,n] = 1/L_{no}[m]$. Furthermore, we assume that $L_{no}[m]$ is the same on the starboard and port sides, i.e., that $L_{no}[-m] = L_{no}[m]$. Then the estimate of $L_{no}[m]$ is obtained as[8]

$$\hat{L}_{no}[m] = \frac{1}{\frac{1}{2N_{\mathcal{N}}}\sum_{n\in\mathcal{N}}(\hat{q}[m,n] + \hat{q}[-m,n])} \quad (11)$$

where $N_{\mathcal{N}}$ is the number of lines in $\mathcal{N}$. In this average the values of $q[m,n]$ from the port and starboard sides are added to cancel out the effect of any yawing in the selected lines. At this point it is not possible to compensate for the effect of pitching or variations in speed on those lines, but this will be done by applying a correction to the estimates of the model parameters in Section IV.

We now multiply the estimates of $q[m,n]$ by $vT_f\hat{L}_{no}[m]$ to obtain estimates of the sampling displacements $|\Delta_n y_s'[m,n]|$,

$$\widehat{|\Delta_n y_s'[m,n]|} = vT_f\hat{L}_{no}[m]\hat{q}[m,n].$$

Detection of Backscanning: Since we have obtained estimates not of the sampling displacements $\Delta_n y_s'[m,n]$, but of their absolute values, it is necessary to detect areas where $\Delta_n y_s'[m,n]$ is negative, i.e., areas where backscanning occurs, and multiply the estimates by -1 in those areas. One possible way of detecting backscanning is to look for areas where objects appear in triplicate. A significant problem with that approach is that it is not always easy to identify these triple images because each pass is made from a different viewing angle and may differ considerably from the others.

A more practical alternative is to look for indications of backscanning in the estimates $\widehat{|\Delta_n y_s'[m,n]|}$ themselves. If we find two neighboring groups of lines of the sonograph where the value of $\widehat{|\Delta_n y_s'[m,n]|}$ is very small on both the starboard and the port side, it is possible that the area between these two groups of lines was backscanned as a result of pitching. Yaw-induced backscanning may have occurred if the value of $\widehat{|\Delta_n y_s'[m,n]|}$ along a line of the sonograph decreases with range until it approaches zero and then starts to increase again. In both cases, visual inspection of the suspected area can confirm whether backscanning actually occurred. In the case of yaw-induced backscanning, since the estimates of sampling displacements are typically very noisy, it was found useful to fit a third-order polynomial to the curve in order to help determine the minimum point. A simple rule that yields

[7] There are only $(N_n - 1)$ unknowns because we are dealing with increments between lines of the image, and the number of increments is one less than the total number of lines, N_n.

[8] As previously noted, the average correlation length is actually a function of l (which represents range) rather than of the horizontal coordinate m. Therefore, the $q[m,n]$ should be added not for fixed m but for values of m corresponding to fixed values of l, according to the slant-range correction at each line. To avoid making the equations more complex, this modification is again left implicit.

good results is to decide that backscanning occurred if the minimum value of the polynomial falls below a threshold chosen so that the number of false alarms and misses is approximately the same, as revealed by visual inspection of the image.

IV. Estimation of Geometric Distortions

In Section III we saw how the sampling displacements $\Delta_n x_s'[m, n]$ and $\Delta_n y_s'[m, n]$ are estimated from the sonograph. We now consider how from those estimates we may in turn estimate the parameters $\Delta x_o'[n]$, $\Delta y_o'[n]$ and $\Delta\theta[n]$ of the linear model derived in Section II and given by (3a) and (3b).

A. Estimation of Model Parameters

For each line of the image the model parameters, $\Delta x_o'[n]$, $\Delta y_o'[n]$, and $\Delta\theta[n]$, are estimated from the estimates of sampling displacements, $\widehat{\Delta_n x_s'}[m, n]$ and $\widehat{\Delta_n y_s'}[m, n]$, on a set of cross-track coordinates $\mathcal{M}[n] = \{m_1[n], m_2[n], \cdots, m_p[n]\}$. These coordinates are chosen from areas where the assumptions of wide-sense stationarity and isotropy appear to be reasonable. Whenever the estimates of sampling displacements reveal pronounced yawing of the towfish it is advisable to choose $\mathcal{M}[n]$ so that the selected columns always come from the side towards which the towfish was turning at the time each line was acquired. In fact, yawing causes the beam to sweep the bottom faster on the opposite side, which may result in undersampling and a consequent loss of accuracy in the estimates of sampling displacements. The side the towfish was turning towards is assumed to be the side with the smallest average value of $\widehat{\Delta_n y_s'}[m, n]$.

The model parameters are estimated separately for each line of the sonograph by deterministic least-squares estimation. This approach may be used in the absence of information about the statistics of the parameters and observation noise. Other alternatives based on recursive stochastic estimation are presented in [20]. The model used for estimating the parameters is

$$\widehat{\Delta_n x_s'}[m, n] = \Delta x_o'[n] + e_x[m, n] \tag{12a}$$

$$\widehat{\Delta_n y_s'}[m, n] = \Delta y_o'[n] + m(cT_s/2)\,\Delta\theta[n] + e_y[m, n] \tag{12b}$$

which corresponds to (3a) and (3b) with additional terms $e_x[m, n]$ and $e_y[m, n]$ that represent the error incurred in replacing $\Delta_n x_s'[m, n]$ and $\Delta_n y_s'[m, n]$ with their estimates.

From (12a) we see that the least-squares estimate of $\Delta x_o'[n]$ is simply the average value of $\widehat{\Delta_n x_s'}[m, n]$. In (12b), we see that $\widehat{\Delta_n y_s'}[m, n]$ is a linear function of m, with coefficients $\Delta y_o'[n]$ and $\Delta\theta[n]$. Therfore, the least squares estimates of $\Delta y_o'[n]$ and $\Delta\theta[n]$ are calculated from $\widehat{\Delta_n y_s'}[m, n]$ through linear regression [22]. We thus have

$$\widehat{\Delta x_o'}[n] = \frac{1}{p[n]} S_x[n]$$

$$\widehat{\Delta y_o'}[n] = \frac{S_{m^2}[n]S_y[n] - S_m[n]S_{my}[n]}{d[n]}$$

$$\widehat{\Delta\theta}[n] = \frac{p[n]S_{my}[n] - S_m[n]S_y[n]}{d[n]}$$

where $p[n]$ is the number of observation points in $\mathcal{M}[n]$ and

$$S_m[n] \triangleq \sum_{m\in\mathcal{M}[n]} m$$

$$S_{m^2}[n] \triangleq \sum_{m\in\mathcal{M}[n]} m^2$$

$$S_x[n] \triangleq \sum_{m\in\mathcal{M}[n]} \widehat{\Delta_n x_s'}[m, n],$$

$$S_y[n] \triangleq \sum_{m\in\mathcal{M}[n]} \widehat{\Delta_n y_s'}[m, n],$$

$$S_{my}[n] \triangleq \sum_{m\in\mathcal{M}[n]} m\widehat{\Delta_n y_s'}[m, n],$$

$$d[n] \triangleq p[n]S_{m^2}[n] - S_m^2[n].$$

The estimates of yaw angle are now calculated by cumulatively adding the increment estimates,

$$\hat{\theta}[n] = \hat{\theta}[0] + \sum_{i=0}^{n-1} \widehat{\Delta\theta}[i].$$

The initial yaw angle estimate, $\hat{\theta}[0]$, is chosen so that the average of $\hat{\theta}[n]$ over the entire sonograph be zero. Notice, however, that the choice of $\hat{\theta}[0]$ does not affect the correction of geometric distortions in the image, but only the orientation of the corrected image as a whole.

Next we obtain estimates of $x_o'[n]$ and $y_o'[n]$ in the (x, y) coordinated system. First, we convert the increments from the (x', y') to the (x, y) coordinate system, through

$$\widehat{\Delta x_o}[n] = \widehat{\Delta x_o'}[n]\cos\hat{\theta}[n] - \widehat{\Delta y_o'}[n]\sin\hat{\theta}[n]$$

$$\widehat{\Delta y_o}[n] = \widehat{\Delta y_o'}[n]\cos\hat{\theta}[n] + \widehat{\Delta x_o'}[n]\sin\hat{\theta}[n].$$

In Section III we mentioned that the estimates of model parameters would have to be corrected to compensate for the effect of pitching and variations in speed on $\hat{L}_{no}[m]$. This is now accomplished by assuming that the average speed with which the sound beam scanned the bottom during the acquisition of the sonograph was equal to the average speed of the towing vessel, v. This assumption implies that the estimates $\Delta y_o[n]$ are to be multiplied by the factor

$$\alpha \triangleq \frac{(N_n - 1)vT_f}{\sum_{n=0}^{N_n-2} \Delta y_o[n]}.$$

To incorporate this correction into the estimates of model

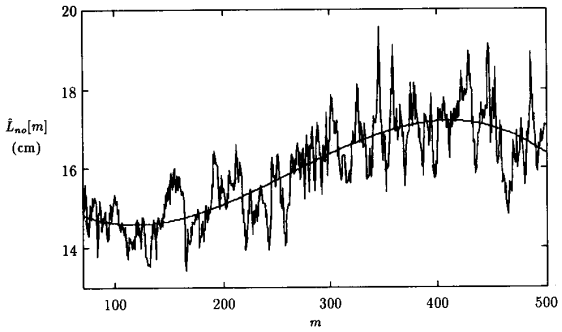

Fig. 14. Average value of $\hat{q}[m, n]$ (rugged line) and estimate of $L_{no}[m]$ (smooth line). The effect of the beam pattern is seen clearly in this curve: it is approxiamtely constant in the near field portion of the beam and then increases linearly with range in the far field, before collapsing as a result of sound absorption by the water as the maximum range of 100 m is approached.

parameters, we recalculate them as

$$\widehat{\Delta x_o'}[n] = \widehat{\Delta x_o}[n] \cos \hat{\theta}[n] + \alpha \widehat{\Delta y_o}[n] \sin \hat{\theta}[n]$$

$$\widehat{\Delta y_o'}[n] = \alpha \widehat{\Delta y_o}[n] \cos \hat{\theta}[n] - \widehat{\Delta x_o}[n] \sin \hat{\theta}[n].$$

B. Estimation of Attitude Parameters

Having estimated the model parameters, we are now ready to correct the geometric distortions in the image. However, before proceeding to describe that operation, we consider briefly how from the estimates of model parameters we can obtain estimates of the towfish attitude parameters themselves. First, the points $(x_o[n], y_o[n])$ are estimated by cumulatively adding the estimates of the increments $\Delta x_o[n]$ and $\Delta y_o[n]$, in the latter case after the correction described at the end of the preceding section. Thus

$$\hat{x}_o[n] = \hat{x}_o[0] + \sum_{i=0}^{n-1} \widehat{\Delta x_o}[i]$$

$$\hat{y}_o[n] = \hat{y}_o[0] + \sum_{i=0}^{n-1} \alpha \widehat{\Delta y_o}[i]$$

with the starting point arbitrarily chosen as the origin of the coordinate system, i.e., $\hat{x}_o[0] = \hat{y}_o[0] = 0$.

From Fig. 7 we see that

$$x_o[n] = x_f[n] - z_f[n] \tan \phi[n] \sin \theta[n] \quad (13a)$$

$$y_o[n] = y_f[n] + z_f[n] \tan \phi[n] \cos \theta[n] \quad (13b)$$

where

$$z_f[n] = h[n] \cos \phi[n]. \quad (14)$$

As previously defined, $h[n]$ is the distance between the towfish and point $(x_o[n], y_o[n])$ and can be measured directly from the sonograph as the height of the water column at each line. These equations are all we have to obtain estimates of $x_f[n]$, $y_f[n]$, $z_f[n]$, and $\phi[n]$ from $h[n]$, $\hat{x}_o[n]$, $\hat{y}_o[n]$, and $\hat{\theta}$[n]. Therefore, it is possible to estimate only two of the attitude parameters, and the third one has to be estimated by different means. One solution to this problem is to assume that the along-track distance between the towfish and the deploying vessel remains constant during the acquisition of the sonograph. That allows $y_f[n]$ to be estimated from navigational measurements of the deploying vessel. If such measurements are not available, it is still possible to resort to the assumption that the

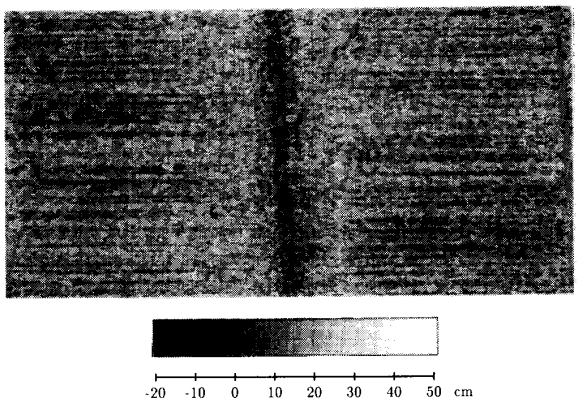

Fig. 15. Estimates of the $|\Delta_n y_s'[m, n]|$ for the sonograph of Fig. 1. The gray level at each point of the image is proportional to the value of $|\Delta_n y_s'[m, n]|$ according to the tone scale shown at the bottom. The variations of the estimates perceived as stripes in the cross-track direction are probably due to yawing of the towfish.

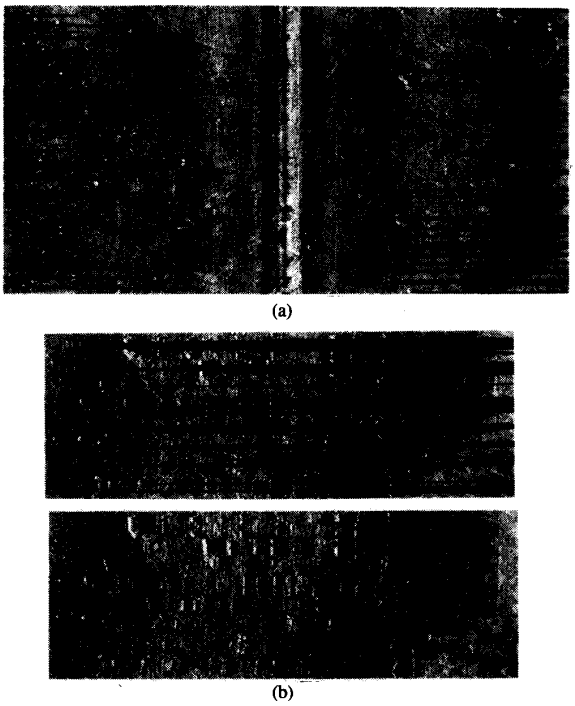

Fig. 16. Areas where backscanning was detected are shown in black (a). The lower right-hand corner is enlarged for comparison with the original sonograph (b). Notice how the algorithm accurately selected the areas where the cable abruptly changes direction as a result of backscanning.

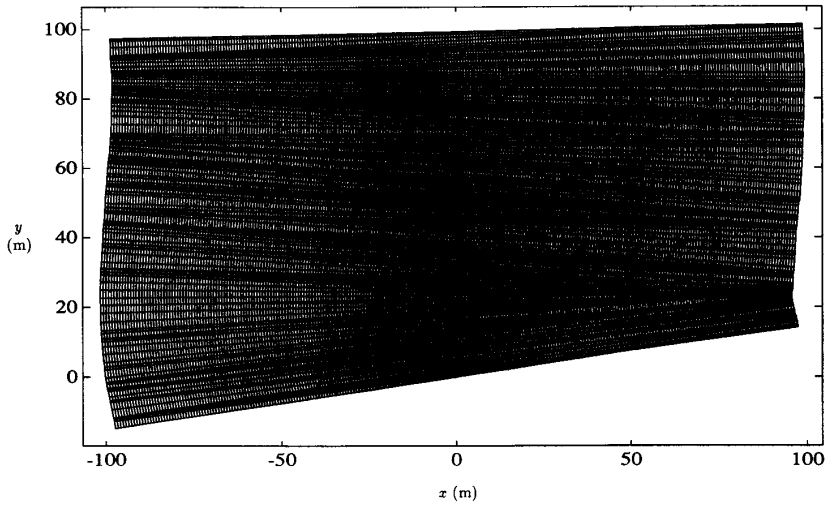

Fig. 17. The estimated sampling points are plotted in a mesh, illustrating the geometric distortion in the sonograph. Plotting every point would make the mesh too dense, and so only every fourth line and column are plotted. This plot provides a picture of how the sonar beam moved across the bottom on the surveyed area, according to our estimates.

towfish moved at a constant speed v, equal to the average speed of the deploying vessel. If $y_f[n]$ is measured, or assumed to satisfy these approximations, (13a), (13b), and (14) may be solved for the remaining attitude parameters, lateral position, $x_f[n]$, and pitch angle, $\phi[n]$. For instance, using the assumption that the towfish moved at a constant speed v, i.e., that

$$\hat{y}_f[n] = nvT_f \tag{15}$$

we obtain from (13b) and (14),

$$\hat{\phi}[n] = \arcsin\left(\frac{\hat{y}_o[n] - nvT_f}{h[n]\cos\hat{\theta}[n]}\right). \tag{16}$$

Finally, from (13a) and (14),

$$\hat{x}_f[n] = \hat{x}_o[n] + h[n]\sin\hat{\phi}[n]\sin\hat{\theta}[n].$$

If measured values of $y_f[n]$ are not available and the approximation of (15) is adopted, then variations in towfish speed from the assumed fixed value v affect the estimates of pitch angle, calculated through (16). Therefore, this equation should be used only with the clear understanding that the resulting estimates $\hat{\phi}[n]$ reflect not only the towfish pitch angle, but also variations in its speed.

C. Estimation of the Sampling Point Coordinates

Returning now to the problem of correcting the geometric distortions in the sonograph, the next step is to obtain estimates of the sampling coordinates, $x_s[m,n]$ and $y_s[m,n]$, for each point of the image, from the estimates of distortion parameter, $\widehat{\Delta x_o'[n]}$, $\widehat{\Delta y_o'}$, and $\widehat{\Delta\theta}[n]$. Using (3a) and (3b), we have

$$\widehat{\Delta_n x_s'}[m,n] = \widehat{\Delta x_o'}[n]$$
$$\widehat{\Delta_n y_s'}[m,n] = \widehat{\Delta y_o'}[n] + m(cT_s/2)\,\widehat{\Delta\theta}[n].$$

These estimates are then converted from the (x', y') to the (x, y) coordinate system through

$$\widehat{\Delta_n x_s}[m,n] = \widehat{\Delta_n x_s'}[m,n]\cos\hat{\theta}[n] - \widehat{\Delta_n y_s'}[m,n]\sin\hat{\theta}[n]$$
$$\widehat{\Delta_n y_s}[m,n] = \widehat{\Delta_n y_s'}[m,n]\cos\hat{\theta}[n] + \widehat{\Delta_n x_s'}[m,n]\sin\hat{\theta}[n].$$

Finally, the estimates of sampling point coordinates are calculated recursively from the estimates of sampling displacements,

$$\hat{x}_s[m,n+1] = \hat{x}_s[m,n] + \widehat{\Delta_n x_s}[m,n]$$
$$\hat{y}_s[m,n+1] = \hat{y}_s[m,n] + \widehat{\Delta_n y_s}[m,n].$$

The initial estimates, $\hat{x}_s[m,0]$ and $\hat{y}_s[m,0]$, $m = 0, \pm 1, \cdots, \pm(N_m - 1)$, are calculated from (2a) and (2b), with $x_o[0] = y_o[0] = 0$ and $\theta[0] = \hat{\theta}[0]$.

The pixels of the sonograph image are now moved to positions corresponding to the estimated locations of the sampling points, and are then interpolated on a rectangular grid to produce the corrected image. For details of this operation, see [20].

V. Examples

Estimates $\widehat{\Delta_n x_s'}[m,n]$ and $\hat{q}[m,n]$ were calculated from the sonograph of Fig. 1 as explained in Section III. For estimation of the sampling displacements, the lines and columns of the image were upsampled by a factor of 16. The normalized sample covariance sequence was calculated over segments 7 pixels long (i.e., $M = 3$), and the threshold used in calculating the correlation lengths was arbitrarily chosen to be $\rho_o = 0.5$. Fig. 14 shows the aver-

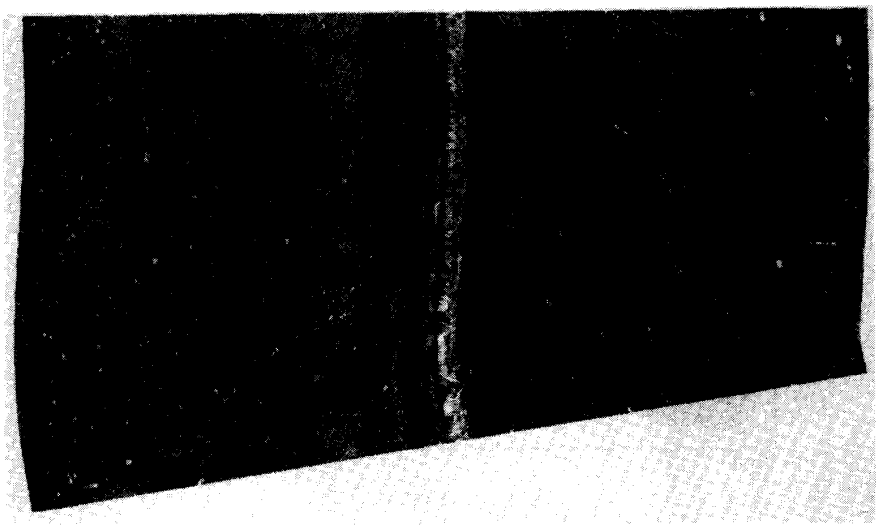

Fig. 18. Sonograph of Fig. 1 after correction of geometric distortions.

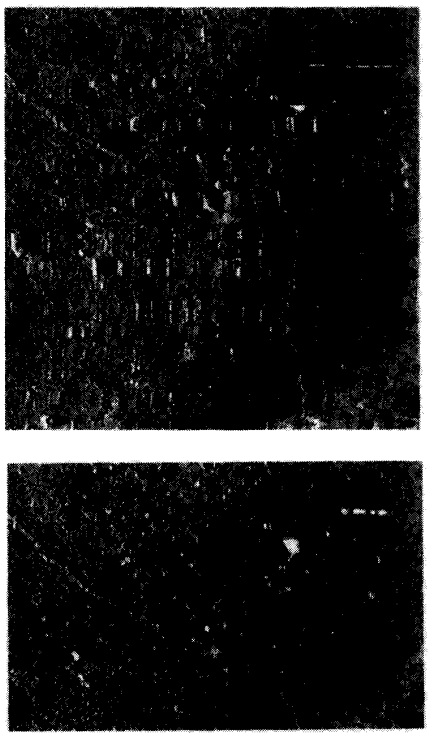

Fig. 19. Comparison of the lower right corner of the sonograph before (top) and after (bottom) correction of the geometric distortions reveals that the cable that appeared pronouncedly jagged as a result of yawing now presents a slowly varying curvature that is most likely closer to its true shape, and that the multiple images of rocks in backscanned areas are correctly replaced by single images.

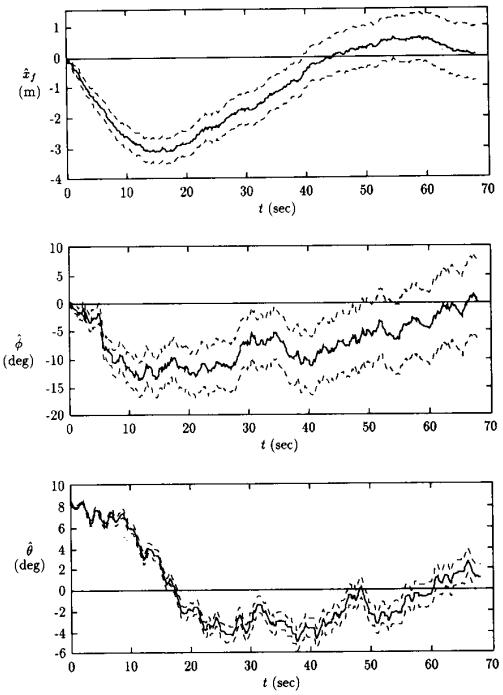

Fig. 20. Estimates of attitude parameters for the sonograph of Fig. 1 with confidence intervals (see explanation in the text). The estimates of yaw angle clearly contain an oscillatory component which is consistent with the swaying of the deploying vessel.

age value of $\hat{q}[m, n]$, calculated from 51 lines (out of a total of 512 lines) that appear to present the least amount of geometric distortion. Since the effect of the beam pattern may be expected to vary smoothly, we fitted a fourth-order polynomial to that average as seen in the figure. This polynomial constituted our estimate of $L_{no}[m]$, which was then multiplied by the $\hat{q}[m, n]$ on the port and starboard sides of each line (remembering that $L_{no}[-m] = L_{no}[m]$), to yield the estimates $\widehat{|\Delta_n y_s'[m, n]|}$.

No patterns could be perceived visually in the estimates of $\Delta_n x_s'[m, n]$, but the estimates of $|\Delta_n y_s'[m, n]|$ show

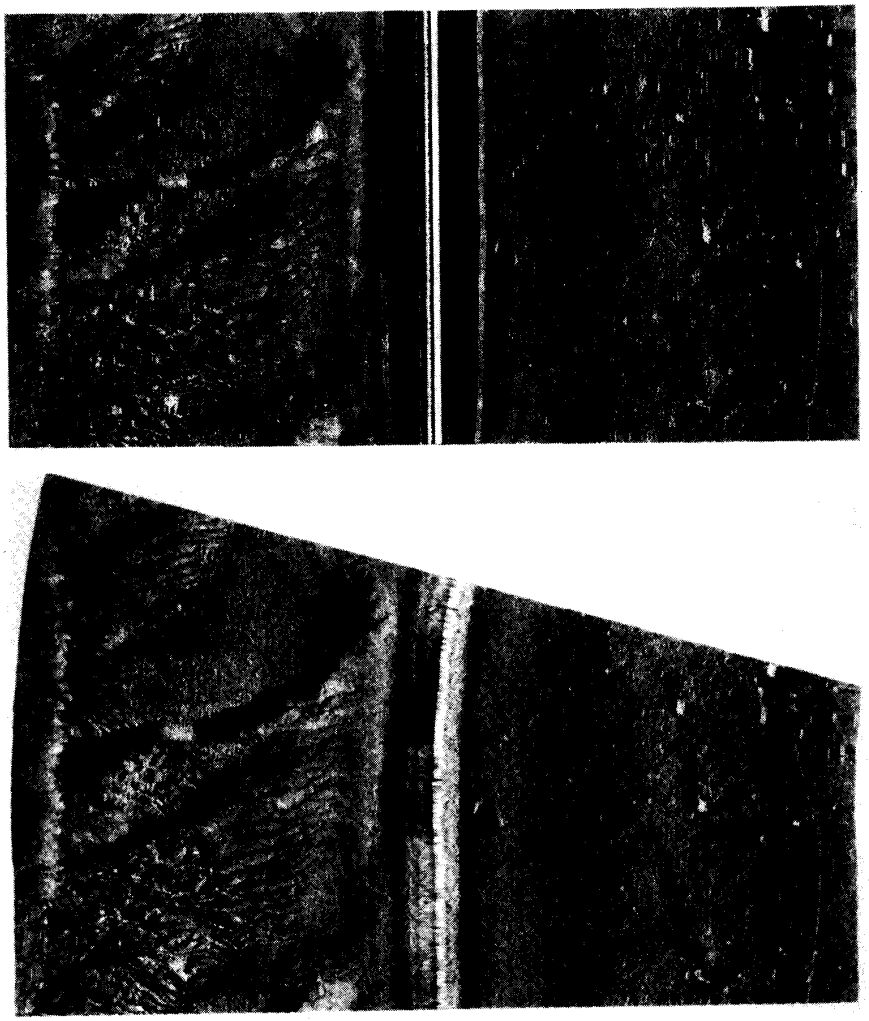

Fig. 21. A second sonograph from our data set, before (top) and after (bottom) correction of geometric distortions. The improvement is most evident in the upper right-hand corner of the image, where features on the bottom appear pronouncedly stretched in the original sonograph, but acquire more natural shapes after processing.

stripes in the cross-track direction that alternate between the port and starboard sides, as seen in Fig. 15. These stripes indicate that the sampling intervals increased and decreased periodically, and the fact that these variations alternate from one side to the other suggests that they were caused by yawing of the towfish induced by swaying of the deploying vessel.

Fig. 16(a) shows the areas in the sonograph where backscanning was detected through the technique discussed in Section III.D. Visual inspection of the original sonograph reveals that all but 40 lines affected by backscanning were correctly detected by the algorithm, while 40 other lines seemingly unaffected were incorrectly selected. Since the total number of lines is 512, we therefore have less than 8% of misses and 8% of false alarms. By multiplying the estimates $\widehat{|\Delta_n y_s'|}[m, n]$ by -1 in the areas where backscanning was detected we obtained the estimates of sampling displacements in the along-track direction, $\widehat{\Delta_n y_s'}[m, n]$.

To estimate the model parameters, we selected every fourth column from columns number 76 to 475 on the side with the smallest average sampling displacement. The number of observations ($p[n] = 100$ for all n) was limited by the resulting memory requirements and execution times of the algorithm. In principle, better results might be obtained with a greater number of observations. The estimates of model parameters were used for calculating the estimates of sampling coordinates through the procedure described in Section IV. A graphic representation of these estimates is obtained by plotting the estimated sampling points $(\hat{x}_s[m, n], \hat{y}[m, n])$ in a mesh, as in Fig. 17.

By resampling the sonograph according to the estimates of sampling coordinates, we obtained the corrected image

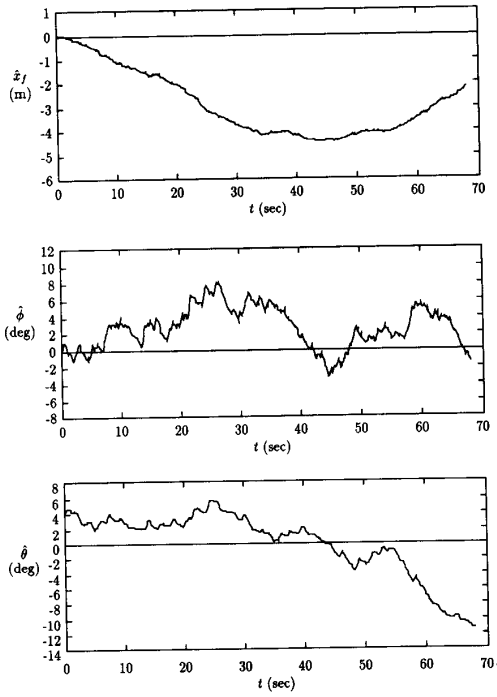

Fig. 22. Estimates of attitude parameters for the sonograph of Fig. 21.

shown in Fig. 18. An enlarged detail of the sonograph before and after correction is shown in Fig. 19. Some areas of this image appear slightly blurred, as a result of aliasing during the acquisition of the original sonograph. That is due to the fact that perfect reconstruction of the image is not possible in areas where the sampling rate in the along-track direction is less than the Nyquist rate of the backscattering function $b(x, y)$, as a result of faster motion of the sonar beam.

Finally, the estimates of attitude parameters calculated from the estimates of model parameters through the procedure described in Section IV.B are shown in Fig. 20. The 95% confidence intervals shown in the figure should be considered only as approximate indicators of the magnitude of the estimation error, since their calculation is complicated by several factors discussed in [20]. Nevertheless, these confidence intervals are useful for indicating relative trends in the evolution of the estimates and in their relative accuracy with respect to one another. For instance, they indicate that, because of the accumulation of the estimation errors of parameter increments, the estimates of attitude parameters become progressively less reliable. In other words, the algorithm is more capable of correcting local geometric distortion than of determining the absolute location of objects in the image. The confidence intervals also indicate that the estimates of yaw angle are more accurate than the estimates of pitch angle.

A second sonograph from our data set is shown in Fig.

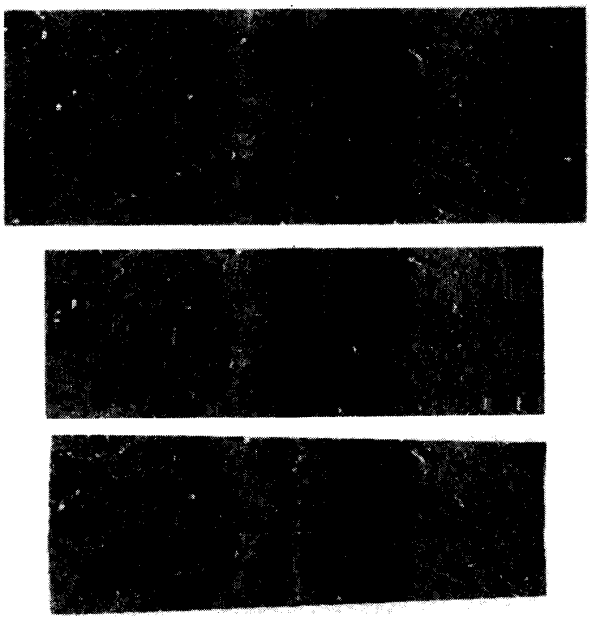

Fig. 23. The image used in the simulation (top) was resampled on an irregular grid over the outlined area to produce a simulated sonograph (middle) that was then processed through our algorithm. Inspection of the corrected image (bottom) reveals considerable reduction of the simulated geometric distortions.

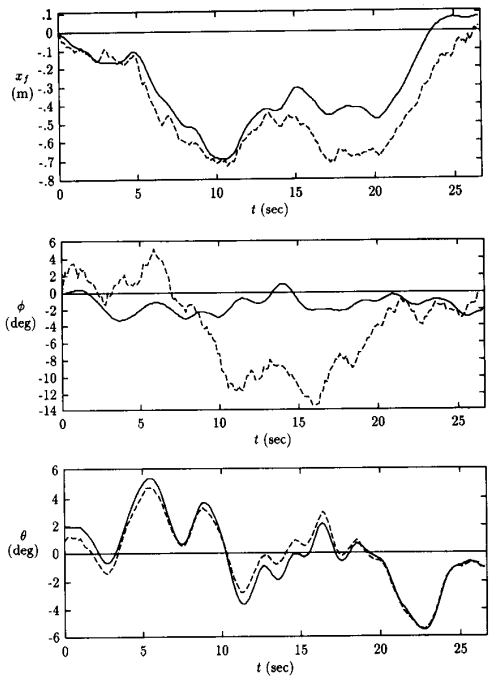

Fig. 24. Simulated (solid lines) and estimated (dashed lines) attitude parameters.

21, before and after correction of the geometric distortions. The estimates of attitude parameters are shown in Fig. 22.

VI. Algorithm Verification Based on Simulation

Precise evaluation of the results obtained with our algorithm would require a photographic mosaic or an extremely detailed bathymetric chart of the surveyed area for comparison with the corrected images. Alternatively, the estimates of attitude parameters could be compared to measurements of their true values obtained with sensors mounted on the towfish. However, sufficiently detailed charts of the surveyed area are not available and the side-scan sonar employed was a common commercial unit, not equipped with attitude sensors. We therefore resorted to a simulation to evaluate the results obtained.

Simulation geometric distortions requires an undistorted image of the seabed that can be resampled in an irregular pattern to simulate the effect of towfish instabilities. Since all the sonographs in our data set present some degree of geometric distortion, it was necessary to artificially generate an image on which to perform the simulation. Such an image was obtained from the corrected sonograph of Fig. 18 after further processing to eliminate the areas affected by blurring, which would be confused by the algorithm with stretching due to geometric distortion. The details of this operation are described in [20]. The image was then resampled on an irregular grid to simulate the production of a sonograph affected by geometric distortions.

Fig. 23 shows the undistorted image and the simulated sonograph, before and after processing by our algorithm. Comparison of the shapes of rocks and scours in the three images shows that the algorithm achieves a significant reduction of the simulated geometric distortions. As pointed out before, perfect reconstruction is not possible in areas where the sampling distance was large enough to cause aliasing.

Fig. 24 shows the simulated attitude parameters used to calculate the sampling coordinates for the production of the simulated sonograph, along with their estimates obtained through our algorithm. The simulated parameters are Gaussian noise sequences with spectra calculated to approximate those of the estimates of attitude parameters previously shown in Fig. 20. Notice that the estimates of yaw angle are rather accurate, with a maximum estimation error of only 1.18°. The estimates of lateral displacement are also considerably accurate, with a maximum error of 28 cm, corresponding to a little more than one pixel in the digitized image. The estimates of pitch angel are less accurate, with a maximum error of approximately 11°. This is explained by the fact that variations in pitch angle produce less geometric distortion than equal variations in yaw angle, because the altitude of the towfish above the seabed is typically only a fraction of the maximum range of the sonar beam.

VII. Conclusions

The main contribution of this article is a procedure for the estimation and correction of geometric distortions in side-scan sonar images without utilizing navigational or towfish attitude measurements. This procedure may be applied to any existing digitized sonographs or to analog sonographs stored on magnetic tape. It is likely to find wider application in the enhancement of sonographs made by high-resolution, high-frequency towfish (roughly, those with operating frequencies of 100 kHz or higher), which are typically not equipped with attitude sensors and are more susceptible to motion instabilities, due to their small size.

In the process of correcting geometric distortions, the algorithm produces other relevant information that can prove useful in the interpretation of sonographs. For instance, it provides a means of detecting lines affected by backscanning, apparently with relatively low percentages of false alarms and misses. It also allows reconstruction of the sampling pattern on the bottom in the form of mesh plots, and provides approximate estimates of the towfish attitude parameters.

Visual inspection of the corrected sonographs offers strong indication that the technique can effectively reduce the degree of geometric distortion, thus fulfilling its main goal. Although the simulation carried out in Section VI does not duplicate all the conditions present in the acquisition of a real sonograph, it does provide some additional evidence of the efficacy of our algorithm. According to that simulation, very accurate estimates of the towfish yaw angle are obtained, as well as fairly accurate estimates of its horizontal lateral displacement.

Future research on the technique presented in this article should encompass further evaluation of its accuracy, perhaps through more extensive simulations. Definitive evaluation, however, can be accomplished by comparing the estimates of attitude parameters with real measurements obtained through attitude sensors mounted on a towfish. Another possibility is to acquire sonographs of areas for which sufficiently detailed bathymetric charts are available, and then attempt to match points in the corrected sonographs with points in the chart. Another issue to be investigated is the feasibility of implementing the algorithm in real time, so that the corrected image may be seen on a display in the deploying vessel as the towfish scans the bottom. Other suggestions for future research on more specific issues related to the algorithm are given in [20].

Acknowledgment

The authors would like to thank Klein Associates, Inc., and the United States Geological Survey for loaning the equipment used for acquiring the sonographs. They also thank Dr. Bruce R. Musicus of Bolt, Beranek and Newman, Inc., and Dr. W. Kenneth Stewart, Jr., of WHOI, for their contribution regarding of the presentation of theo-

retical results, and the reviewers of the paper for their many useful comments.

REFERENCES

[1] M. L. Somers and A. R. Stubbs, "Sidescan sonar," *Proc. Inst. Elec. Eng.*, vol. 131, pp. 243–256, June 1984.

[2] A. R. Stubbs, "Identification of patterns of asdic records," *Int. Hydrogr. Rev.*, vol. 40, pp. 53–68, 1963.

[3] B. W. Flemming, "Causes and effects of sonograph distortion and some graphical methods for their manual correction," in *Recent Developments in Side Scan Sonar Techniques*, W. G. A. Russell-Cargill, Ed. South Africa: Central Acoustics Laboratory, Univ. Cape Town, 1982, ch. 5, pp. 103–138.

[4] P. S. Chavez, Jr., "Processing techniques for digital sonar images from GLORIA," *Photogrammetric Eng. Remote Sens.*, vol. 52, pp. 1133–1145, Aug. 1986.

[5] B. W. Flemming, "Side-scan sonar: A practical guide," *Int. Hydrogr. Rev.*, vol. 53, pp. 65–92, Jan. 1976.

[6] C. S. Clay and H. Medwin, *Acoustical Oceanography.* New York: Wiley, 1977.

[7] P. N. Denbigh and B. W. Flemming, "Range prediction and calibration in side scan sonar," in *Recent Developments in Side Scan Sonar Techniques*, W. G. A. Russell-Cargill, Ed. South Africa: Central Acoustics Laboratory, Univ. Cape Town, 1982, ch. 4, pp. 81–100.

[8] P. R. Paluzzi *et al.*, "Computer rectification and mosaicking of side-looking sonar images," in *Proc. 13th Annual Offshore Technology Conf.*, pp. 103–114, May 1981.

[9] B. P. Luyendyk, E. J. Hajic, and D. S. Simonett, "Side-scan sonar mapping and computer-aided interpretation in the Santa Barbara Channel, California," *Marine Geophysical Researches*, vol. 5, pp. 365–388, 1983.

[10] J.-M. Augustin, "Side scan acoustic images processing software," in *Proc. 1986 Working Sym. Oceanographic Data Syst.*, pp. 221–228, Feb. 1986.

[11] E. Clerici, "Evaluation of relative effectiveness of some image processing techniques applied to side-scan sonar data," in *Proc. US–Australia Workshop on Image Processing Techniques for Remote Sensing*, pp. 1–10, May 1978.

[12] D. B. Prior, J. M. Coleman, and L. E. Garrison, "Digitally acquired undistorted side scan sonar images of submarine landslides, Mississippi River delta," *Geology*, vol. 7, pp. 423–425, Sept. 1979.

[13] M. Ennis and J. W. J. van Wick, "Image processing on side scan sonar records," in *Proc. Fourth South African Symp. Digital Image Processing*, pp. 83–93, July 1986.

[14] C. Eaves-Walton and G. A. Shippey, "Digital image processing for sidescan sonar data analysis," in *Fifth Int. Conf. Electronics for Ocean Technology*, pp. 203–209, Mar. 1987.

[15] T. B. Reed, IV and D. Hussong, "Digital image processing techniques for enhancement and classification of SeaMARC II side scan sonar imagery," *J. Geophys. Res.*, vol. 94, pp. 7469–7490, June 1989.

[16] M. Shishido and K. Naito, "A study on picture improvement for side looking sonar—Part 1," *NEC Research & Development*, pp. 62–74, Apr. 1979.

[17] P. G. Teleki *et al.*, "Sonar survey of the U.S. atlantic continental slope; acoustic characteristics and image processing techniques," in *Proc. 13th Annual Offshore Technology Conf.*, pp. 91–102, May 1981.

[18] W. K. Stewart, Jr., "Multisensor modeling underwater with uncertain information," Ph.D. dissertation, Massachusetts Institute of Technology, Cambridge, MA, July 1988.

[19] D. Jan and J. Minot, "Les traitements d'image en sonar latéral," *L'Onde Électrique*, vol. 69, pp. 13–19, May/June 1989.

[20] D. T. Cobra, "Estimation and correction of geometric distortions in side-scan sonar images," Ph.D. dissertation, Mass. Inst. of Technology and Woods Hole Ocean. Inst., Mar. 1990. (Also published as Tech. Rep. RLE TR-556, May 1990, and WHOI-90-25, Aug. 1990.)

[21] T. K. Stanton, "Sonar estimates of seafloor microroughness," *J. Acoust. Soc. Am.*, vol. 75, pp. 809–818, Mar. 1984.

[22] P. R. Bevington, *Data Reduction and Error Analysis for the Physical Sciences.* New York: McGraw-Hill, 1969.

Daniel T. Cobra (S'89–M'90) received the degree of electrical engineer form the Universidade de Brasília, Brazil, in 1983, the M.S. degree from the Massachusetts Institute of Technology, Cambridge, MA, in 1986, and a joint Ph.D. degree in electrical engineering from M.I.T. and in oceanographic engineering from the Woods Hole Oceanographic Institution, Woods Hole, MA, in 1990.

Since June 1990 he has been an Adjunct Professor at the Departamento de Engenharia Elétrica of the Universidade de Brasília, Brazil. His main area of research is digital signal processing and its applications to image processing and underwater, aerial, and satellite remote sensing.

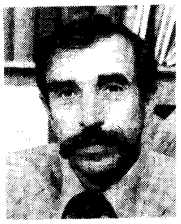

Alan V. Oppenheim (S'57–M'65–SM'71–F'77) received the S.B. and S.M. degrees in 1961 and the Sc.D. degree in 1964, all in electrical engineering, from the Massachusetts Institute of Technology, Cambridge, MA.

In 1964 he joined the faculty at M.I.T., where he is currently Distinguished Professor of electrical engineering. From 1978 to 1980 he was Associate Head of the Data Systems Division at M.I.T. Lincoln Laboratory. Since 1977, he has also been a Guest Investigator at the Woods Hole Oceanographic Institution, Woods Hole, MA. He is the author of several widely used textbooks on digital signal processing.

Dr. Oppenheim has been a Guggenheim Fellow, a Sackler Fellow, and has held the Cecil H. Green distinguished chair in Electrical Engineering and Computer Science. He has also received a number of awards for outstanding research and teaching, including the 1988 IEEE Education Medal, and is an elected member of the National Academy of Engineering. He is also a member of Tau Beta Pi, Eta Kappa Nu, and Sigma Xi.

Jules S. Jaffe (A'85) received the B.A. degree from the State University of New York at Buffalo in physics in 1973, the M.S. degree in biomedical information science from the Georgia Institute of Technology, Atlanta, in 1974, and the Ph.D degree in biophysics from the University of California, Berkeley, in 1982.

After spending several years working in industry as an Image-Processing Consultant, he joined the Woods Hole Oceanographic Institute as a Pew Memorial Fellow in 1984 at the Assistant Scientist level, and was promoted to Associate Scientist in 1988. He is currently an Assistant Research Oceanographer at the Scripps Institution of Oceanography, Marine Physical Laboratory, University of California at San Diego, which he joined in 1988. His research interests are in the areas of image reconstruction and restoration, with a special emphasis on three-dimensional systems. He is currently designing underwater optical and sonar imaging systems for ocean exploration.